Passive control of instabilities in combustion systems with heat exchanger

Aswathy Surendran[1], Maria A Heckl[1], Naseh Hosseini[2,3] and Omke Jan Teerling[3]

Abstract

One of the major concerns in the operability of power generation systems is their susceptibility to combustion instabilities. In this work, we explore whether a heat exchanger, an integral component of a domestic boiler, can be made to act as a passive controller that suppresses combustion instabilities. The combustor is modelled as a quarter-wave resonator (1-D, open at one end, closed at the other) with a compact heat source inside, which is modelled by a time-lag law. The heat exchanger is modelled as an array of tubes with bias flow and is placed near the closed end of the resonator, causing it to behave like a cavity-backed slit plate: an effective acoustic absorber. For simplicity and ease of analysis, we treat the physical processes of heat transfer and acoustic scattering occurring at the heat exchanger as two individual processes separated by an infinitesimal distance. The aeroacoustic response of the tube array is modelled using a quasi-steady approach and the heat transfer across the heat exchanger is modelled by assuming it to be a heat sink. Unsteady numerical simulations were carried out to obtain the heat exchanger transfer function, which is the response of the heat transfer at heat exchanger to upstream velocity perturbations. Combining the aeroacoustic response and the heat exchanger transfer function, in the limit of the distance between these processes tending to zero, gives the net influence of the heat exchanger. Other parameters of interest are the heat source location and the cavity length (the distance between the tube array and the closed end). We then construct stability maps for the first resonant mode of the aforementioned combustor configuration, for various parameter combinations. Our model predicts that stability can be achieved for a wide range of parameters.

1. Introduction

In order to combat pollution and to reduce NO_x emissions in combustion systems like gas turbine engines, industrial burners, domestic boilers etc., lean premixed combustion is used, i.e. the fuel and air are fully mixed prior to combustion. However, such combustion systems are susceptible to combustion instability or thermoacoustic instability.

Combustion instability is a consequence of the interactions between the heat source, flow and acoustics, of which thermoacoustic instability occurs due to the presence of positive feedback between the unsteady heat release rates and the acoustic oscillations. The latter is characterised by large amplitude, low-frequency self-excited oscillations that can be detrimental. If unchecked, these instabilities can cause vibrations of mechanical parts, unsteady and enhanced heat fluxes to walls and concentrated thermal and pressure loads leading to fatigue and in extreme cases severe structural damage.

[1]School of Chemical and Physical Sciences, Keele University, Staffordshire, UK
[2]Department of Mechanical Engineering, Eindhoven University of Technology, Eindhoven, The Netherlands
[3]Bekaert Combustion Technology BV, The Netherlands

Corresponding author:
Maria Heckl, Keele University Keele University, Keele, Staffordshire ST5 5BG, UK.
Email: m.a.heckl@keele.ac.uk

To eliminate thermoacoustic instabilities, the feedback loop between the unsteady heat release rate and the acoustic fluctuations must be broken. This can be done in two ways: by use of either active or passive control strategies. In active control, the operating conditions of the systems are modified through external means. These involve continuous monitoring of the system with time and modifying the system parameters dynamically, to prevent instabilities from arising. Reviews on active control of combustion instabilities can be found in Candel[1] and McManus et al.,[2] who provide a broad overview of the underlying mechanisms of combustion instabilities and some active control principles.

In contrast to active control, the passive control strategies do not have a dynamic component. Their behaviour is fixed in time. These strategies include changes to hardware and other design modifications like changes to combustion chamber geometry or the injector geometry, inclusion of acoustic dampers, or even changes in the reactant composition. Some of the most commonly used passive control components are Helmholtz resonators, quarter-wave and half-wave tubes, baffles. These control units modify the acoustic pressure field within the combustion system, thereby avoiding any feedback loop between the acoustic and heat release rate oscillations.

Even though these passive control strategies are all viable control options in large power generation units, especially stationary ones,[3] they are impractical in small and compact units like domestic boilers. One of the main differences between the gas turbine engines or other large power generators and small power generation units like domestic boilers, is the presence of heat exchangers in the latter. In a domestic boiler, the heat exchanger (*hex*) is housed within the combustion chamber along with the flame, and so requires no additional space. With this as the basis, we propose to use heat exchangers as a viable alternative to control thermoacoustic instabilities in combustion systems like domestic boilers.

Heat exchangers are periodic structures that consist of arrays of tubes in a cross flow. It is evident from literature survey that tube rows or tube banks in cross flow can effectively damp acoustic oscillations. Some of the relevant works are mentioned below. If sound passes through an array of tubes, it is attenuated due to viscous, thermal and turbulent losses. We aim to utilise this attenuation property of tube arrays to control thermoacoustic instabilities.

Kristiansen and Fahy[4,5] have developed a simple theory for the prediction of sound dissipation in tube banks subjected to steady cross flow. They treated the tube bank as a special homogeneous medium whose characteristic properties or parameters were determined from the mean flow data. They observed that the attenuation within the tube bank increased with increasing mean flow velocity.

Quinn and Howe[6] derived the dispersion relation for sound propagation through a bank of rigid circular tubes in cross flow. They observed that the attenuation of sound increases with decreasing Strouhal number. In other words, for a given incident acoustic frequency and tube diameter, the sound attenuation increases with increasing mean cross flow velocity. However, the approach by Quinn and Howe utilises a highly idealised flow modelling and hence provides only a qualitative description of the acoustic behaviour of the tube bank.

As an approximation, one may also treat the heat exchanger tube row as an array of thin sharp-edged rods with rectangular cross section, as shown by Surendran and Heckl.[7,8] They modelled the heat exchanger tube row as a slit-plate and examined the passive control capability of this configuration on an idealised combustion system. Slit-plates and orifice structures are widely used as acoustic absorbers, especially in room acoustics,[9] and their acoustic absorption can be enhanced to a great extent by the inclusion of a cavity backing.[10]

Experimental and theoretical studies have also been carried out in the area of thermoacoustic instability control using cavity-backed perforated plates with bias flow. Experimental studies done by Tran et al.[11,12] showed the successful implementation of a cavity-backed perforated plate, to annul the thermoacoustic instability in a swirl combustor. This work was extended by Scarpato et al.[13,14] who studied the influence of Strouhal number on the damping behaviour of the perforated plate. Stability predictions of Tran's combustor were carried out by Heckl and Kosztin,[15] using a Green's function approach. By modelling the flame dynamics through a generic heat release rate law, they investigated the effective control of instabilities by varying the cavity lengths and the time-lags (in the heat release rate law).

In combustion systems like domestic boilers, the heat exchanger transfers the heat produced within the combustion chamber to the coolant being circulated around, and then to radiators. Hence, the heat exchanger acts as the heat sink and is bound to have a significant effect on the thermoacoustic stability of the combustion system. One of the earliest researchers to investigate this effect are Bosscha,[16] Riess[17] and Raun et al.[18] They placed a cold wire gauze in the top half of a Rijke tube and observed amplified pressure oscillations while the wire gauze was being heated by a flame. In a more recent study, Rigas et al.[19] experimentally verified the use of an unheated mesh as a drag-inducing device, to control thermoacoustic instability in

an electrically heated Rijke tube. They measured both growth rates and eigenfrequencies, and also obtained stability maps for the system, while varying the heater power and the location of the control mesh. Hosseini et al.[20] have treated the heat exchanger as an active acoustic element in a combustion system (Rijke tube) and examined its effect on the stability of the system by varying the time delays in the heat source and heat sink, the temperature jumps across the heat source/sink as well as the distance between the heat sink and the heat source. An analytical investigation of the effects of heat transfer and area change on the acoustics of a simplified combustion chamber consisting of a duct and a convergent-divergent nozzle was conducted by Hosseinalipour et al.[21] They observed that heat absorption or cooling along the duct and the nozzle had significant influence on the acoustic reflection and transmission i.e., increase in cooling was observed to subside the reflection while promoting transmission.

The aim of the present work is to investigate the passive control capability of heat exchangers and to use them effectively to suppress the thermoacoustic instability in an idealised domestic boiler system, by tuning the downstream acoustic properties of the combustion system. Our combustor is modelled as a quarter-wave resonator with a compact heat source. The heat exchanger is located near the closed end (downstream) of the resonator, causing it to behave like a cavity-backed tube row. The influence of hex on the stability of the combustor is examined through its aeroacoustic response to the incoming acoustic fluctuations as well as its heat transfer response to the upstream velocity fluctuations. We also take into account the jumps in mean temperature across both the heat source and the heat exchanger. In order to examine the instability control potential of the cavity-backed heat exchanger, we undertake a stability analysis by constructing stability maps for a wide range of hex properties.

Our paper is structured as follows: The detailed description of the combustion system with underlying assumptions are given in Section 2, where the modelling aspects of the heat source is also given. Section 3 and Section 4 pertain to the modelling of the heat exchanger and the derivation of the acoustic properties of the cavity-backed hex respectively. In Section 5, we look at the influence of some of the system parameters on the acoustic properties of the cavity-backed hex. We then proceed to the stability predictions (Section 6) for various system parameters, using eigenvalue method, drawing conclusions for the stability behaviour from Section 5.

2. Description of the system

The domestic boiler configuration is simplified to its basic components consisting of the burner, the heat exchanger and its outer casing. Further simplifications to our modelling are:

– We discard the fuel-air mixture and exhaust gas compositions. Instead, we assume a homogeneous medium encompassing the burner and the hex, having different mean temperature values at different regions within the boiler.
– The hex is assumed to be maintained at a constant temperature of 340 K.
– Even though the geometrical complexities in a real boiler calls for modelling a duct with varying area of cross section, in our simplified case, we have assumed a duct with constant area of cross section.

After all these simplifying assumptions, the modelled combustion system reduces to that of a quarter-wave resonator with both heat source (flame) as well as heat sink (hex) as shown in Figure 1. The open end at $x = 0$ acts as an inlet for the unburnt fuel-air mixture and the closed end denotes the outer casing of the boiler. The open end is characterised by its reflection coefficient $R_0 = -1$ and the closed end by the corresponding reflection coefficient of $R_p = 1$. We are treating the downstream end of the combustor as a piston in order to vary the distance between the hex and the backing wall. This distance is referred to as the cavity length (l_c) and is one of the key parameters in our study. The heat source, which denotes the flame front at the burner, is located at a distance $x = l_f$ from the upstream end, dividing the resonator into a cold upstream region (Region 1) and a hot downstream region (Region 2). The speeds of sound $(c_{1,2})$ and mean temperatures $(\bar{T}_{1,2})$ are uniform in both regions, where $\bar{T}_1 < \bar{T}_2$ and subsequently $c_1 < c_2$. The hex is located at a distance $x = L$ from the open end.

2.1. Acoustic field

The acoustic waves within the combustion system are assumed one-dimensional and propagating perpendicular to the hex tubes (normal incidence). They consist of
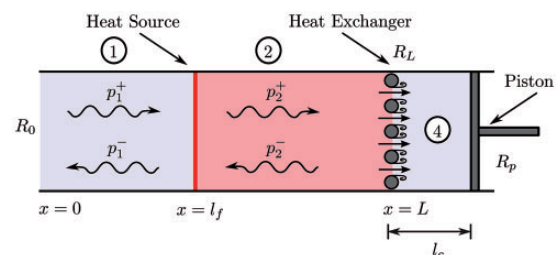

Figure 1. Schematic of the modelled combustion system.

forward (p^+) and backward (p^-) travelling waves, with amplitudes A_1 and B_1 respectively, in Region 1, and amplitudes A_2 and B_2 respectively, in Region 2. The acoustic pressure and velocity fields within the combustion system are denoted as

$$p_r(x) = p_r^+ + p_r^- = A_r e^{ik_r(x-l_f)} + B_r e^{-ik_r(x-l_f)} \quad (1)$$

$$u_r(x) = u_r^+ + u_r^- = \frac{1}{\rho_r c_r}\{p_r^+ - p_r^-\} \quad (2)$$

where p^+ and p^- are the forward and backward travelling pressure waves respectively, A and B are the pressure amplitudes and u^+ and u^- are the acoustic velocities corresponding to p^+ and p^- respectively. The subscript 'r' denotes the region within the combustor, ω is the frequency of the acoustic wave, ρ is the density of the fluid and $k_r = \omega/c_r$ is the wave number in the region 'r'. In our analysis, the mean flow velocity is very small ($\sim \mathcal{O}(1\text{m/s})$) compared to the speed of sound and hence can be neglected in the mathematical formulation. The factor $e^{-i\omega t}$ is omitted throughout the analysis.

2.2. Heat source

In typical burners, the heat source is the surface stabilised flame front composed of multiple flames. However, the lengths of individual flames are much smaller than the acoustic wavelengths encountered within the combustion system. Therefore, the heat source in our idealised combustion system can be assumed as a compact and planar sheet, confined to an infinitesimally thin region at $x = l_f$. The heat release rate fluctuation ($\hat{Q}_f$) is assumed to follow the simple $n - \tau$ form of time-lag law, where it depends on the time-lagged acoustic velocity fluctuations at $x = l_f$ i.e.;

$$\hat{Q}_f(x, \omega) = nu_1(x)e^{i\omega\tau}\delta(x - l_f) \quad (3)$$

Here, τ is the time-lag and n is the interaction index. Using equation (2), $\hat{Q}_f(x, \omega)$ can be expressed in terms of the acoustic pressure as

$$\hat{Q}_f(x, \omega)|_{x=l_f} = n\, e^{i\omega\tau} \frac{(p_1^+ - p_1^-)}{\rho_1 c_1} \quad (4)$$

3. Heat exchanger modelling

The thermoacoustic interactions occurring at the hex can be regarded as an overall effect of two physical processes. The first process is the heat transfer response of the hex, and the second process is the aeroacoustic
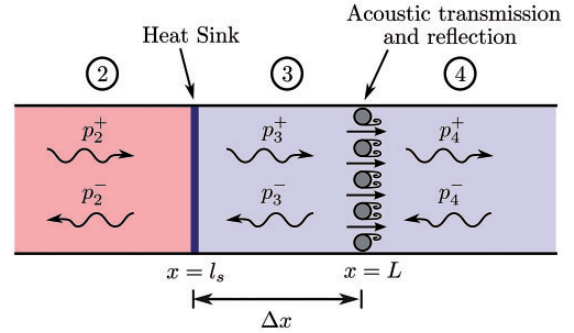
Figure 2. Schematic of the heat exchanger acting as both heat sink and acoustic scatterer.

response of the hex to incoming velocity perturbations, which is modelled as the acoustic scattering by the hex. In the former case, we treat the hex as a heat sink and then model the heat transfer response as the interactions between the fluctuations of heat absorption rate and incoming velocity fluctuations.

For simplicity and ease of analysis, we treat these two physical processes i.e., heat absorption and acoustic scattering, at the hex as two individual and independent processes separated by an infinitesimal distance Δx as shown in Figure 2. We also assume that the heat transfer phenomenon precedes the acoustic scattering and occurs at $x = l_s$, while the acoustic scattering occurs at $x = L$. Once the individual processes are modelled independent of each other, we can derive the net response of the hex by combining the heat transfer and aeroacoustic responses (similar to network modelling approach) and by letting $\Delta x \rightarrow 0$.

3.1. Model for heat sink

The heat absorption rate fluctuation at the hex, due to the incoming velocity fluctuation, was obtained using the transfer function approach mentioned in Hosseini et al.[22] Numerical simulations for the heat absorption or heat transfer response of the hex were conducted using the transient CFD solver ANSYS FLUENT® 15.0. on the geometry shown in Figure 3. Rather than modelling an array of circular tubes, we have limited the computational domain to that of a semi-circular tube and half the gap height, with symmetry boundary conditions on either sides. At the inlet and outlet, '*velocity inlet*' and '*pressure outlet*' boundary conditions were imposed, respectively. A 2-D, laminar and incompressible flow was assumed in the computational domain. The hex was maintained at a constant temperature of 340 K whereas the incoming flow was at 1500 K. Simulations were conducted for diameter $d = 3\,\text{mm}$, open area ratio $\eta = 0.1$ and inlet velocities
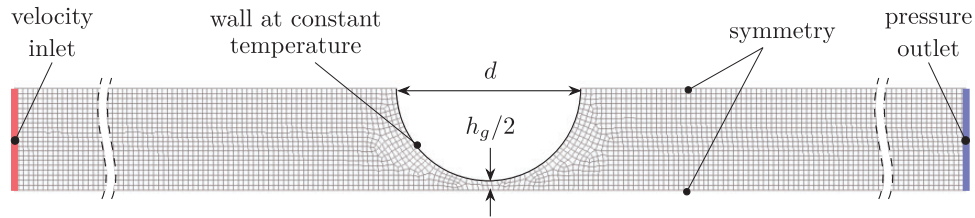
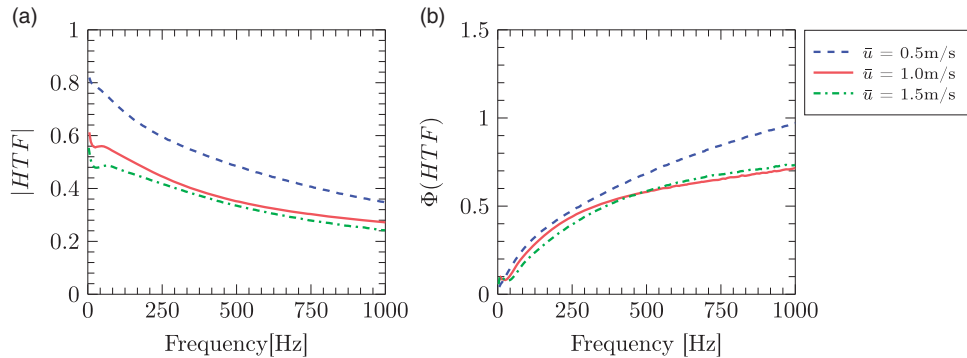**Figure 3.** Meshed geometry with boundary conditions.

Figure 4. (a) |HTF| and (b) Φ(HTF) obtained from numerical simulations, for $d = 3$ mm, $h_g = 0.3$ mm and different mean velocities, $\bar{u}$.

0.5, 1.0 and 1.5 m/s. Open area ratio (η) is the ratio of the gap height h_g to the diameter d.

3.1.1. Transfer function approach. For applying the transfer function approach, a step perturbation in the inlet velocity was chosen. The total velocity in the domain after the introduction of the step perturbation will be $u(t) = \bar{u} + u'(t)$, where $\bar{u}$ is the mean velocity at the inlet and $u'(t)$ is the step perturbation. The magnitude of the perturbation was chosen to be very small, as small as $|u'| = 5\%$ of $\bar{u}$. This is to avoid any nonlinearities in the system. The heat transfer occurring at the hex is recorded and is given by $Q_h(t) = \bar{Q}_h + Q'_h(t)$. Here, $\bar{Q}_h$ is the mean heat absorption rate at the hex and Q'_h is the change in the heat absorption rate due to the velocity perturbation $u'(t)$.

For a constant temperature condition at the hex surface, the heat flux to the wall from the fluid cell is computed as $q'_h = h_f (T_w - T_f)$, where q'_h is the local heat flux, h_f is the fluid-side local heat transfer coefficient, T_w is the wall temperature and T_f is the local fluid temperature. The total heat flux, Q'_h, is evaluated by integrating q'_h over the hex surface. In the simulations, the flow was assumed to be inviscid. However, the specific heat capacity at constant pressure (C_p) was assumed to be a piecewise polynomial in temperature, causing the Prandtl number in the flow domain to have values in the range 0.74–0.9.

The transient simulations give the time response of the hex in terms of the heat absorbed at the hex. The time step Δt is 10^{-5} s and the sampling frequency used (F_s) is 10^5 Hz. Steady flow simulation was conducted initially and then this steady state solution was used as an input to evaluate the transient behaviour of the hex before applying the step forcing. This method was used to get faster convergence for the transient behaviour. Nevertheless, around 500 to 1000 time steps were allowed to lapse before the step forcing was applied. After applying the step, the simulation was continued till the system attained a new stationary state where the changes to the system properties over time were minimal.

To relate the response of the hex to the velocity input, we convert the time data to their corresponding frequency responses through Fourier transformation, i.e. $u'(t) \xrightarrow{FT} \hat{u}(\omega)$ and $Q'_h(t) \xrightarrow{FT} \hat{Q}_h(\omega)$. The heat exchanger transfer function is then calculated using the equation given below.

$$\text{HTF} = \frac{\hat{Q}_h / \bar{Q}_h}{\hat{u} / \bar{u}} \quad (5)$$

HTF is a complex quantity with both magnitude |HTF|, and phase Φ(HTF), and it depends on the flow field, geometry and frequency of the incoming perturbation. |HTF| is also referred to as the gain of HTF. Typical gain-phase plots of HTF of a hex are shown in Figure 4(a) and (b). The hex has diameter $d = 3$ mm and open area ratio $\eta = 0.1$. The incoming velocities are $\bar{u} = 0.5$, 1.0 and 1.5 m/s. The gain-phase plots suggest
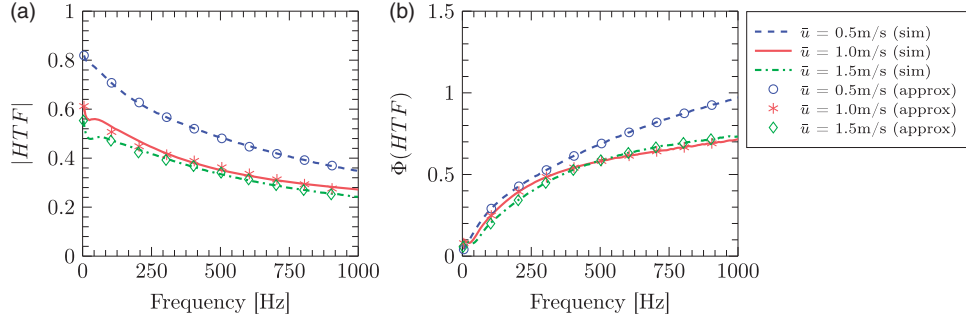
Figure 5. Comparison of |HTF| and Φ(HTF) obtained from numerical simulations (curves) with their approximations (markers), for $d = 3$ mm, $h_g = 0.3$ mm and different mean velocities, $\bar{u}$.

that the hex acts like a low-pass filter i.e., the gain decreases with increasing frequency. We observe that for all values of $\bar{u}$ considered in this study, the starting value of |HTF| is less than 1,[23–25] and it decreases with increasing $\bar{u}$.

Given the HTF, we can now construct a $\hat{Q} - \hat{u}$ relationship, similar to that of a heat source, from equation (5) as

$$\hat{Q}_h = \left\{|HTF|e^{i\Phi(HTF)}\right\}\frac{\hat{u}}{\bar{u}}\bar{Q}_h \qquad (6)$$

Therefore, it is necessary to obtain mathematical expressions for HTF.

3.1.2. Approximations to transfer functions.
The mathematical expressions for the gain and phase of the HTF were obtained by assuming trial functions in the form of polynomials, and determining the coefficients of these trial functions using a constrained least squares approach.[26] For the HTF shown in Figure 4, we have assumed the following trial functions.

$$\log(|HTF|) = \begin{cases} a_0 + a_1 f + a_2 f^2 + a_3 f^3 & f \le f_p \\ b_0 + b_1\sqrt{f} & f \ge f_p \end{cases} \qquad (7)$$

$$\Phi(HTF) = \begin{cases} e_0 + e_1 f + e_2 f^2 + e_3 f^3 + e_4 f^4 & f \le f_p \\ g_0 + g_1\sqrt{f} + g_2 f + g_3\left(\sqrt{f}\right)^3 + g_4 f^2 & f \ge f_p \end{cases} \qquad (8)$$

where a_m, b_m, e_m and g_m are the coefficients to be determined. Constraints are imposed at the first frequency (f_0) value and an intermediate frequency (f_p) value. The markers in Figure 5(a) and (b) show the approximated |HTF| and Φ(HTF) along with the simulated data (shown as curves). Here, f_p is 500 Hz for the approximation of |HTF| and 200 Hz for the approximation of Φ(HTF). We can observe that except for a slight deviation in the initial slope of |HTF|, the approximated function accurately captures the simulated data.

Substituting equations (7) and (8) into equation (6) and taking $\hat{u}$ to be the acoustic velocity fluctuation upstream of $x = l_s$, we obtain

$$\hat{Q}_h = \left(u_2^+ + u_2^-\right)\left(\bar{Q}_h/\bar{u}_2\right)\left\{|HTF|e^{i\Phi(HTF)}\right\} \qquad (9)$$

3.2. Model for acoustic scattering

The acoustic scattering at the hex is modelled using a quasi-steady approach. Quasi-steady modelling was previously utilised by Ronneberger[27] in studying the effect of subsonic mean flow on the aeroacoustic response of a stepwise expansion in a pipe or a sudden area expansion, and then by Hofmans et al.[28,29] and Durrieu et al.[30] in studying the response of a diaphragm or a slit-plate in a pipe.

To proceed with the modelling, we first simplify the geometry of the tube row by approximating it to two half cylinders placed within a duct. The half cylinders are separated by a gap (h_g) and have a bias flow through the gap (u_g) (see Figure 3). The Mach number corresponding to this bias flow is denoted by M_g and is defined as $M_g = u_g/c_3$, where c_3 is the speed of sound in Region 3. We assume that

– there is no temperature change across the tube row ($\bar{T}_3 = \bar{T}_4$), and the speed of sound is uniform across the Regions 3 and 4 ($c_3 = c_4$),
– the tube row is very compact compared to the acoustic wavelength, and that there are no phase changes to the acoustic quantities across the source/sink region,
– the flow within the duct is assumed to be inviscid and compressible (unless stated otherwise) and the incoming Mach number is very low i.e., $M_3 \ll 1$, in order to maintain a subsonic flow through the gap ($M_g < 1$).

The flow within the duct is divided into three regions: (a) Region 3 – uniform flow upstream of the
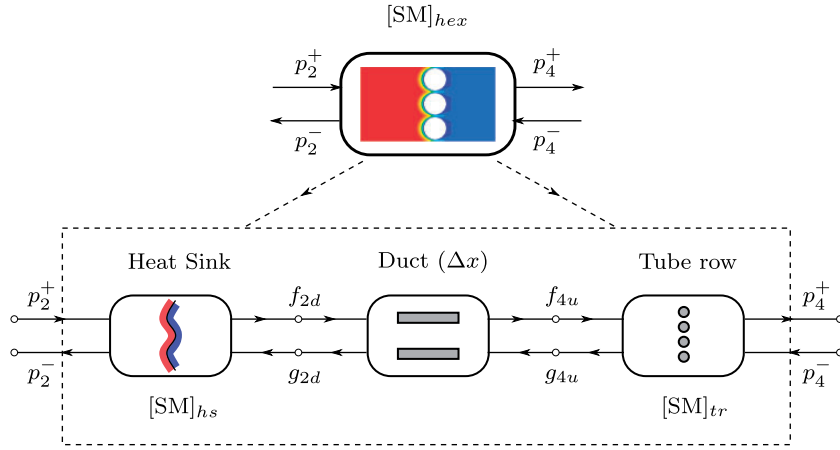
Figure 6. Schematic of the network modelling approach used on hex.

tube row, (b) a compact source/sink region around the tube row, where acoustic energy could be produced or dissipated due to vortex shedding, and (c) Region 4 – uniform flow downstream of the tube row. We make use of the conservation equations for mass (continuity), momentum and energy across different regions to derive the scattering matrix of the given tube row. The scattering matrix relates the enthalpy perturbations upstream of the sample to the enthalpy perturbations downstream. The procedure followed in obtaining the scattering matrix is similar to that given in literature.[31–33] Surendran et al.[32] have analytically derived and experimentally validated the scattering matrix, for both tube row and half cylinders, in the presence/absence of bias flow.

The scattering matrix for a case with no incoming entropy is derived as

$$\begin{bmatrix} (1+M_4)p_4^+ \\ (1-M_3)p_3^- \end{bmatrix} = \begin{bmatrix} T_t^+ & R_t^- \\ R_t^+ & T_t^- \end{bmatrix} \begin{bmatrix} (1+M_3)p_3^+ \\ (1-M_4)p_4^- \end{bmatrix} \quad (10)$$

where M is the Mach number. p^+ and p^- denote the forward and backward travelling pressure waves, R and T denote the reflection and transmission coefficients of the approximated geometry and the superscripts '+' and '–' for R and T denote the upstream and downstream properties respectively. The subscript 't' stands for tube row. The '$\pm$' notation for the coefficients should not be mistaken with those used for the forward and backward travelling waves. The scattering matrix, in this case, is the matrix whose elements are $T_t^\pm$ and $R_t^\pm$.

3.3. Total scattering matrix of hex

The total scattering matrix, $[SM]_{hex}$, of the heat exchanger is obtained by using a network modelling approach.

In this approach, the physical processes of heat transfer and acoustic scattering, occurring at the hex, are treated as independent phenomena, separated by an infinitesimally small distance Δx, as shown in Figure 6. Each phenomenon is modelled as a frequency response, in the form of a two-input-two-output system that maps the outgoing acoustic pressure waves to the incoming acoustic pressure waves. This mapping is represented by the corresponding scattering matrix $[SM]$. Therefore, the total scattering matrix of the hex can be written as

$$\begin{bmatrix} p_4^+ \\ p_2^- \end{bmatrix} = \underbrace{\begin{bmatrix} T_{u\rightarrow d} & R_d \\ R_u & T_{d\rightarrow u} \end{bmatrix}}_{[SM]_{hex}} \begin{bmatrix} p_2^+ \\ p_4^- \end{bmatrix} \quad (11)$$

and the scattering matrices of the individual processes as

$$\begin{bmatrix} f_{2d} \\ p_2^- \end{bmatrix} = \underbrace{\begin{bmatrix} T_h^+ & R_h^- \\ R_h^+ & T_h^- \end{bmatrix}}_{[SM]_{hs}} \begin{bmatrix} p_2^+ \\ g_{2d} \end{bmatrix} \quad (12)$$

for the heat sink, and

$$\begin{bmatrix} p_4^+ \\ g_{4u} \end{bmatrix} = \underbrace{\begin{bmatrix} T_t^+ & R_t^- \\ R_t^+ & T_t^- \end{bmatrix}}_{[SM]_{tr}} \begin{bmatrix} f_{4u} \\ p_4^- \end{bmatrix} \quad (13)$$

for the tube row. Here f_{2d} and f_{4u} are the forward travelling waves downstream of heat sink and upstream of tube row, respectively. Similarly, g_{2d} and g_{4u} are the backward travelling waves downstream of heat sink and upstream of tube row, respectively.

The scattering matrix of the heat sink, $[SM]_{hs}$, is obtained by matching the acoustic fields across

the heat sink i.e.,

$$p_2^+ + p_2^- = f_{2d} + g_{2d} \quad \text{(pressure continuity)} \quad (14)$$

$$\frac{1}{\rho_3 c_3}[f_{2d} - g_{2d}] - \frac{1}{\rho_2 c_2}[p_2^+ - p_2^-] = \frac{(\gamma - 1)}{\rho_2 c_2^2 S}\hat{Q}_h \quad (15)$$

(velocity jump).

Substituting equation (9) in equation (15), we obtain the velocity jump condition in terms of the approximated HTF as

$$f_{2d} - g_{2d} = \zeta_{32}(1 + \alpha)[p_2^+ - p_2^-] \quad (16)$$

where

$$\zeta_{32} = \frac{\rho_3 c_3}{\rho_2 c_2} \quad (17)$$

and

$$\alpha = \frac{(\gamma - 1)\bar{Q}_h\{|\text{HTF}|e^{i\Phi(\text{HTF})}\}}{(\rho_2 c_2^2 S)\bar{u}_2} \quad (18)$$

In our work, we name α as the *heat sink coefficient*. ζ_{32} is the ratio of impedances across the heat sink. $\zeta_{32} = 1$ for $\bar{T}_2 = \bar{T}_3$ and $\zeta_{32} > 1$ for $\bar{T}_2 > \bar{T}_3$. After some algebraic manipulations involving equations (14)–(18), we can derive the elements of $[\text{SM}]_{hs}$ as

$$T_h^+ = \frac{2\,\zeta_{32}(1 + \alpha)}{1 + \zeta_{32}(1 + \alpha)} \quad (19)$$

$$R_h^+ = \frac{\zeta_{32}(1 + \alpha) - 1}{1 + \zeta_{32}(1 + \alpha)} \quad (20)$$

$$T_h^- = \frac{2}{1 + \zeta_{32}(1 + \alpha)} \quad (21)$$

$$R_h^- = \frac{1 - \zeta_{32}(1 + \alpha)}{1 + \zeta_{32}(1 + \alpha)} \quad (22)$$

The scattering matrix of the tube row, $[\text{SM}]_{tr}$, is found from the quasi-steady model (equation (10)), and the pressure field within the duct of length Δx is given by

$$f_{4u} = f_{2d}e^{(ik_3 \Delta x)} \quad (23)$$

$$g_{4u} = g_{2d}e^{(-ik_3 \Delta x)} \quad (24)$$

From equations (12), (13), (23) and (24), we can evaluate the elements of the total scattering matrix of the hex as[34]

$$T_{u \to d} = \frac{T_h^+ T_t^+ e^{(ik_3 \Delta x)}}{1 - R_h^- R_t^+ e^{(2ik_3 \Delta x)}} \quad (25)$$

$$R_u = R_h^+ + \frac{T_h^+ T_h^- R_t^+ e^{(2ik_3 \Delta x)}}{1 - R_h^- R_t^+ e^{(2ik_3 \Delta x)}} \quad (26)$$

$$T_{d \to u} = \frac{T_h^- T_t^- e^{(ik_3 \Delta x)}}{1 - R_h^- R_t^+ e^{(2ik_3 \Delta x)}} \quad (27)$$

$$R_d = R_t^- + \frac{T_t^+ T_t^- e^{(2ik_3 \Delta x)}}{1 - R_h^- R_t^+ e^{(2ik_3 \Delta x)}} \quad (28)$$

In the limit $\Delta x \to 0$, the elements of the scattering matrix reduce to

$$T_{u \to d} = \frac{T_h^+ T_t^+}{1 - R_h^- R_t^+} = \frac{2\,\zeta_{32}(1 + \alpha)\,T_t^+}{(1 - R_t^+) + \zeta_{32}(1 + \alpha)(1 + R_t^+)} \quad (29)$$

$$R_u = R_h^+ + \frac{T_h^+ T_h^- R_t^+}{1 - R_h^- R_t^+} = \frac{(R_t^+ - 1) + \zeta_{32}(1 + \alpha)(1 + R_t^+)}{(1 - R_t^+) + \zeta_{32}(1 + \alpha)(1 + R_t^+)} \quad (30)$$

$$T_{d \to u} = \frac{T_h^- T_t^-}{1 - R_h^- R_t^+} = \frac{2\,T_t^-}{(1 - R_t^+) + \zeta_{32}(1 + \alpha)(1 + R_t^+)} \quad (31)$$

$$R_d = R_t^- + \frac{T_t^+ T_t^-}{1 - R_h^- R_t^+} = R_t^- + \frac{T_t^+ T_t^- [1 - \zeta_{32}(1 + \alpha)]}{(1 - R_t^+) + \zeta_{32}(1 + \alpha)(1 + R_t^+)} \quad (32)$$

4. Cavity-backed heat exchanger

Since the hex is placed near the closed downstream end of the combustor, the effective acoustic property of the downstream end will include the influence of the cavity backing. Hence, the reflection coefficient R_L at $x = L$ is the effective reflection coefficient of the hex and the cavity backing. It is the ratio of the reflected pressure wave p_2^- to the incident wave p_2^+. Using equation (11) and the reflection coefficient of R_p at $x = L + l_c$ i.e., $p_4^- = R_p\, e^{(2ik_4 l_c)}\, p_4^+$, we can derive the effective reflection coefficient as[35]

$$R_L = R_u + \frac{T_{d \to u}\, T_{u \to d}\, R_p\, e^{2ik_4 l_c}}{1 - R_d\, R_p\, e^{2ik_4 l_c}} \quad (33)$$

Special cases are $R_p = 1$ (piston) and $R_p = -1$ (open end).

In our study, we aim to effectively use a cavity-backed hex to dampen or suppress thermoacoustic instability. To quantify the damping property of the cavity-backed hex configuration, we introduce a quantity known as the absorption coefficient (Δ_L), which is the ratio of the acoustic energy absorbed or dissipated

by the cavity-backed hex to the incident acoustic energy. It is defined as

$$\Delta_L = 1 - |R_L|^2 \tag{34}$$

Δ_L can take two extreme values, 1 or 0, depending on the reflection behaviour of the cavity-backed hex. In one case, $|R_L| = 1$ indicates that the cavity-backed hex may behave as a closed end ($R_L = 1$) or as an open end ($R_L = -1$), leading to no absorption i.e., $\Delta_L = 0$ of the incident sound. In the other case, $|R_L| = 0$ indicates an anechoic condition and there will be maximum absorption of the incident sound, i.e. $\Delta_L = 1$. So, for the cavity-backed hex to be an efficient acoustic damper, Δ_L must be maximised.

5. Parameter study

From equations (29) to (32), we can infer that the total scattering property of the hex depends on

- α, which is influenced by the frequency of the incoming wave (f), the incoming velocity ($\bar{u}_2$) and the temperature jump across the hex ($\bar{T}_2 - \bar{T}_3$);
- $[SM]_{tr}$, which is influenced by the hex tube diameter (d), open area ratio (η), the velocity in Region 3 ($\bar{u}_3$); and
- ζ_{32}, which is a measure of the temperature jump across the hex.

5.1. Influence of heat sink coefficient (α)

To study the influence of α on $[SM]_{hex}$, we plot the elements of the total scattering matrix for the three velocities, by first assuming $\alpha = 0$ and then comparing it with the results obtained using data from numerical simulations, where $\alpha \neq 0$. These results are plotted in Figure 7. The solid markers are obtained from numerical simulations with $\alpha \neq 0$ and the curves (with hollow markers) are evaluated for $\alpha = 0$, both using equations (29)–(32).
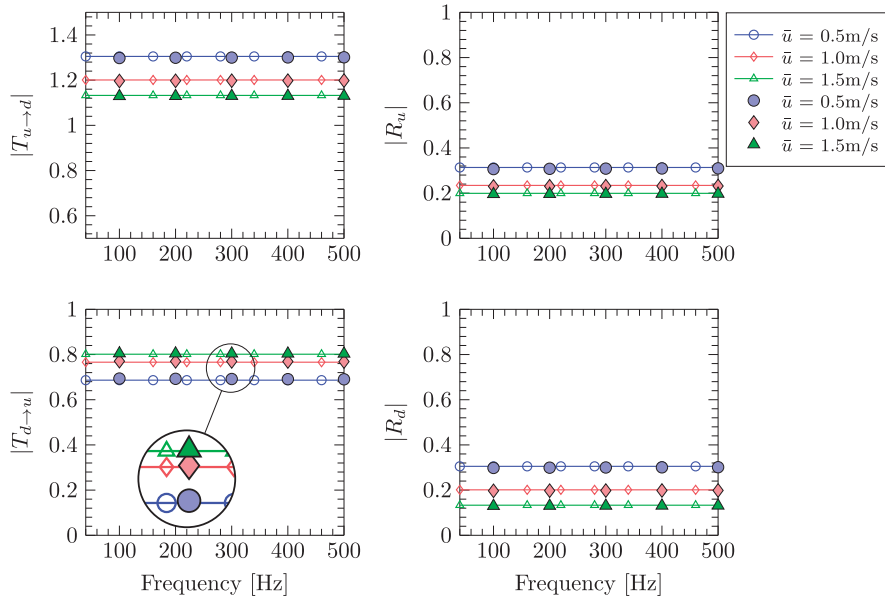
The results plotted show that the influence of α on the scattering elements is negligible (refer to zoomed region in Figure 7). Therefore, for the purpose of parametric analysis, α can be neglected, leading to the simplification of equation (29)–(32) to

$$T_{u \to d} = \frac{2 \, \zeta_{32} \, T_t^+}{\left(1 - R_t^+\right) + \zeta_{32}\left(1 + R_t^+\right)} \tag{35}$$

$$R_u = \frac{\left(R_t^+ - 1\right) + \zeta_{32}\left(1 + R_t^+\right)}{\left(1 - R_t^+\right) + \zeta_{32}\left(1 + R_t^+\right)} \tag{36}$$

$$T_{d \to u} = \frac{2 \, T_t^-}{\left(1 - R_t^+\right) + \zeta_{32}\left(1 + R_t^+\right)} \tag{37}$$

$$R_d = R_t^- + \frac{T_t^+ \, T_t^- \, \left(1 - \zeta_{32}\right)}{\left(1 - R_t^+\right) + \zeta_{32}\left(1 + R_t^+\right)} \tag{38}$$

Figure 7. Variation of the elements of $[SM]_{hex}$ as a function of frequency (f), for fixed velocities, $d = 3$ mm and $\eta = 0.1$. Solid markers indicate the results obtained by including α and curves indicate the results obtained by using $\alpha = 0$.

The plots also indicate that the frequency has minimal influence on the scattering matrix. The magnitudes of the continuous curves remain as constants for the frequency range considered, indicating a quasi-steady response. Here, we can observe that $|T_{u \to d}|$ is greater than 1, while $|T_{d \to u}|$ is less than 1, and this behaviour is caused by the temperature jump across the hex (see discussion in Section 5.2). Similar results were obtained by Strobio Chen et al.,[34] where the scattering matrix of the hex was evaluated numerically using OpenFOAM®. The transmission and reflection coefficients were evaluated for the acoustic velocity, and this resulted in $|T_{u \to d}|$ being less than 1 and $|T_{d \to u}|$ being greater than 1 in Strobio Chen et al.[34]

5.2. Influence of impedance ratio (ζ_{32})

The influence of ζ_{32} on the scattering properties of the hex is as shown in Figure 8. The curves and markers are calculated for hex of $d = 3$ mm, $\eta = 0.1$, $f = 100$ Hz and $\bar{u} = 0.5$, 1.0 and 1.5 m/s. The solid markers indicate results from numerical simulations ($\alpha \neq 0$) and the curves indicate those results when $\alpha = 0$ (equations (35)–(38)). As mentioned in the previous section, the value of the scattering matrix do not vary drastically due to the omission of α.

In the limit of $\alpha \to 0$, the acoustic matching conditions across the heat sink reduce to that of pressure continuity. Hence, the heat sink can be treated as an interface between the hot medium in Region 2 and the cold medium in Region 3. There is a sudden change in

the impedance across the heat sink which causes increasing values (>1) for $|T_{u \to d}|$ as ζ_{32} is increased. Also, R_d becomes increasingly negative as ζ_{32} is increased, and this causes the trend reversal in $|R_d|$ compared to $|R_u|$.

From numerical simulations, it is evident that $\bar{T}_3$, and subsequently ζ_{32}, vary with the incoming velocity $\bar{u}_2$, for a given geometry of tube row (d and η) (Figure 8). The $\bar{T}_3$ and the corresponding ζ_{32} values obtained from the numerical simulations, for $d = 3$ mm, $\eta = 0.1$ and $\bar{T}_2 = 1500$ K are shown in Table 1.

For the purpose of parametric analysis, we assume a constant temperature of $\bar{T}_3 = 400$ K ($\zeta_{32} = 1.936$) across the hex. This assumption does not affect the trends exhibited in the variation of the scattering matrix elements with respect to other parameters. Therefore, the set of assumptions used in the parametric analysis are

- The influence of α is ignored i.e., $\alpha = 0$
- The variation of ζ_{32} with respect to $\bar{u}_2$ is ignored
- The values of $\bar{T}_3$ and ζ_{32} used in the parametric analysis are 400 K and 1.936, respectively

5.3. Influence of cavity backing and resonance (l_c)

It can be confirmed from equation (33) that in addition to the acoustic scattering properties of the hex, the cavity length (l_c) also influences the effective reflection and absorption properties of the cavity-backed hex.
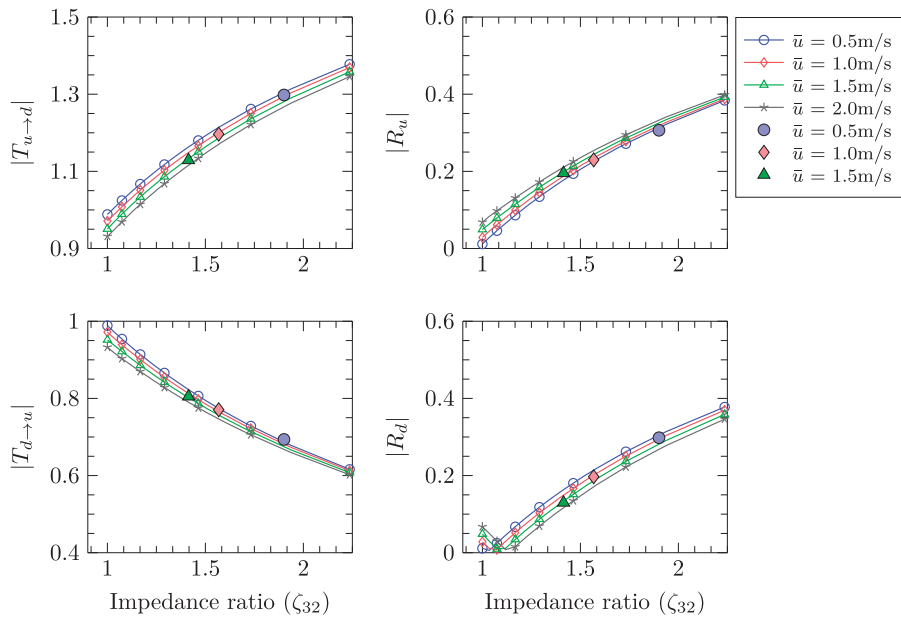
Figure 8. Variation of the elements of $[SM]_{hex}$ as a function of ζ_{32}, for fixed velocities, $f = 100$ Hz, $d = 3$ mm and $\eta = 0.1$. Solid markers indicate the results obtained by including α and curves indicate the results obtained by using $\alpha = 0$.

Here, the cavity backing can act as an additional resonator, causing resonance or anti-resonance, depending on the downstream reflection coefficient R_p.

Studies conducted on slit-plates backed by a rigid plate ($R_p = 1$) have shown that for an incident acoustic wave of frequency f, there will be maximum absorption if the cavity length $l_c = c_4/(4f)$,[10] where c_4 is the speed of sound inside the cavity. Similarly, for the cavity-backed hex, it can be observed from Figure 9(b) that for a particular frequency, the maximum absorption (Δ_L) is experienced for that l_c value which is equal to the quarter wavelength of the incident frequency. The absorption can be enhanced if $\bar{u}$ is increased, as will be studied in Section 5.5. $|R_L|$, on the other hand, exhibits a trend opposite to that of Δ_L. It decreases while Δ_L

increases and vice versa. A maximum for $|R_L|$ indicates resonance behaviour, and a minimum for $|R_L|$ indicates an anti-resonance behaviour. In the latter situation, the cavity-backed hex acts as a near-anechoic end and is favoured for acoustic damping. The plots given in Figure 9 are for $R_p = 1$, with frequencies $f = 100$, 200, 300 and 400 Hz, $d = 3$ mm, $\eta = 0.1$, $\bar{u} = 2.0$ m/s and $\zeta_{32} = 1.936$.

5.4. Influence of frequency (f)

In Figure 7 (from Section 5.1), it can be noted that the acoustic response of the hex on its own does not have any explicit dependence on frequency, at least in the frequency range where quasi-steady model holds. But, the inclusion of a cavity drastically changes the acoustic response of the cavity-backed hex. The influence of frequency on the reflection and absorption coefficients of a cavity-backed hex are shown in Figure 10. It can be observed that $|R_L|$ decreases with increasing f, reaches a minimum and then increases, whereas Δ_L increases with increasing f, attains a maximum and then decreases. The depth of the minimum in $|R_L|$ and the height of the maximum in Δ_L are both increased as the flow velocity is increased. Also, these minimal and maximal values in $|R_L|$ and Δ_L respectively, fall in the same

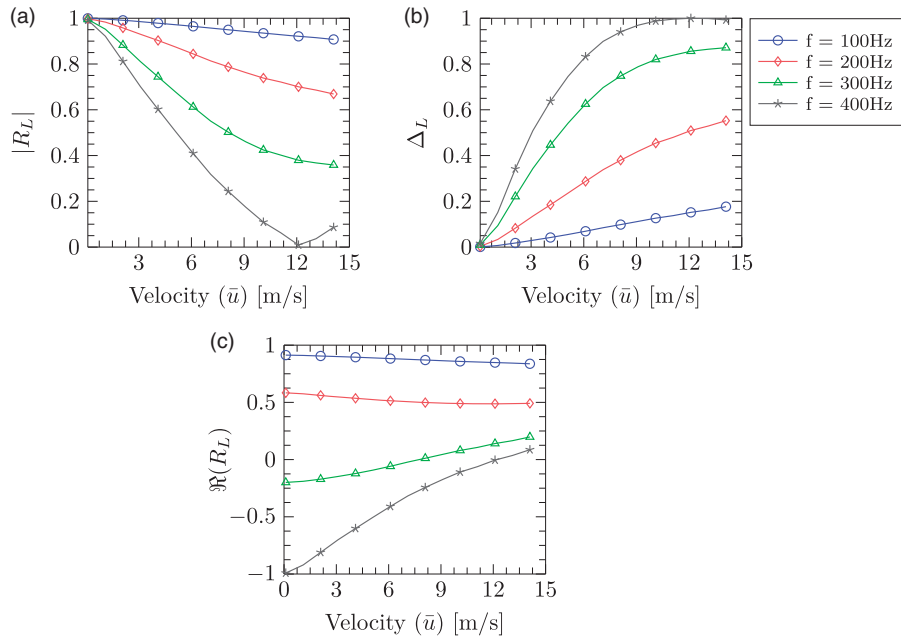**Table 1.** $\bar{T}_3$ and ζ_{32} for $d = 3$ mm and $\eta = 0.1$, evaluated from numerical simulations.

$\bar{u}_2$ (m/s)	$\bar{T}_3$ (K)	ζ_{32}
0.5	415	1.901
1.0	610	1.568
1.5	750	1.414
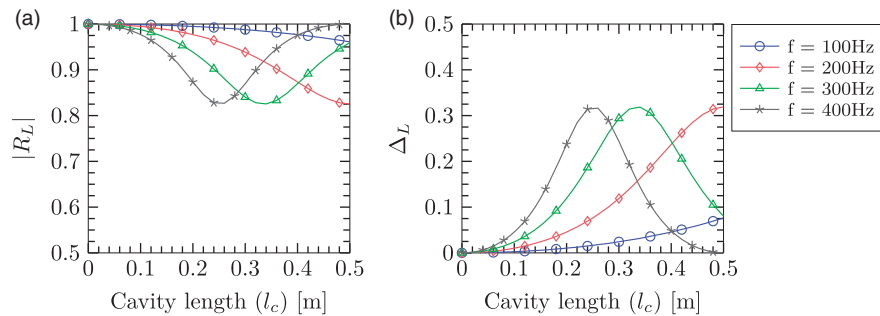
Figure 9. Variation of $|R_L|$ and Δ_L as functions of the cavity length (l_c), for fixed frequencies, $d = 3$ mm, $\eta = 0.1$, $\zeta_{32} = 1.936$, $R_p = 1$ and $\bar{u} = 2.0$ m/s.
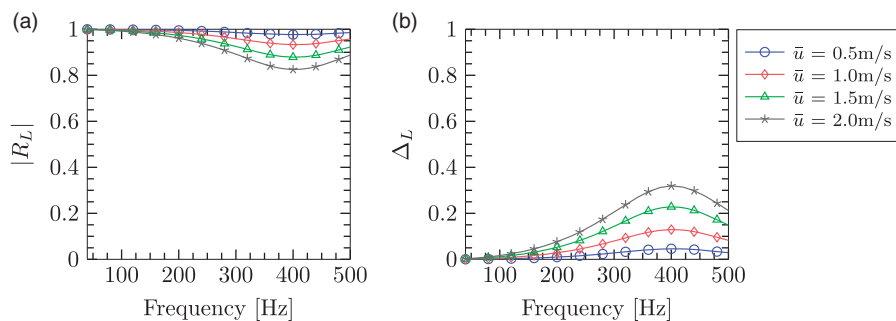
Figure 10. Variation of $|R_L|$ and Δ_L as functions of frequency (f), for fixed velocities, $d = 3$ mm, $\eta = 0.1$, $\zeta_{32} = 1.936$ and $l_c = 0.25$ m.

Figure 11. Variation of $|R_L|$, Δ_L and $\Re(R_L)$ as functions of the mean flow velocity ($\bar{u}$), for fixed frequencies, $d=3$ mm, $\eta=0.1$, $\zeta_{32}=1.936$ and $l_c=0.25$ m.

frequency range for the various velocities considered. This shows that for a given l_c, d, η and ζ_{32}, the damping associated with the frequencies in a particular range can be enhanced by increasing $\bar{u}$. For the plots in Figure 10, $l_c=0.25$ m, $d=3$ mm, $\eta=0.1$ and $\zeta_{32}=1.936$.

5.5. Influence of mean flow velocity ($\bar{u}$)

Figure 11 shows the variation of $|R_L|$, Δ_L and the real part of R_L denoted by $\Re(R_L)$, as functions of the mean flow velocity, for four fixed frequencies: $f=100$, 200, 300 and 400 Hz, $d=3$ mm, $\eta=0.1$, $l_c=0.25$ m and $\zeta_{32}=1.936$. From Figure 11(a), we can observe that for increasing values of $\bar{u}$, $|R_L|$ decreases, reaches a minimum and then increases. In Figure 11(b), Δ_L increases with increasing $\bar{u}$, attains a maximum and then decreases.

One may, by intuition, expect that an increase in $\bar{u}$ indicates an increase in the perceived *blockage* experienced by the flow (due to compressibility and boundary layer effects), leading to an increase in the effective reflection. This trend is not shown in Figure 11(a), but the real part of R_L depicts this trend (Figure 11(c)). The presence of cavity causes R_L to have values between -1 (open end) and $+1$ (closed end). For some frequencies like 100 Hz, the cavity-backed hex behaves like a rigid or an almost rigid end with $R_L>0$ and close to $+1$. For other frequencies like 400 Hz, whose peaks in Δ_L are close to 1, the increase in $\bar{u}$ causes R_L to start out as an open termination (R_L close to -1), and then gradually proceeds to an almost closed termination (R_L tending to 1). At a critical velocity, for a given frequency, R_L becomes 0, causing the cavity-backed hex to behave as an anechoic end. This condition favours the maximum absorption of the incident sound.

6. Stability analysis of the combustor

A linear stability analysis of the combustor configuration (Figure 1) considered in this work is carried out through the use of stability maps that depict the stable and unstable regimes of the combustor for different system parameters. In our analysis, we have described the combustion system in the frequency domain, and hence we use the classical eigenvalue method to predict the eigenfrequencies of the combustion system, and to construct the stability maps. We evaluate the eigenfrequencies of a system by formulating the characteristic equation (from a system of homogeneous equations), and subsequently solving it to get its roots.

6.1. Boundary and jump conditions

The combustion system can now be reduced to a configuration consisting of a duct which is open at one end ($R_0=-1$ at $x=0$) and having a reflection coefficient of R_L at the other end ($x=L$). R_L is the effective reflection coefficient of the cavity-backed hex. The heat source is located at a distance of $x=l_f$ from the open end.

When formulating the characteristic equation for our combustor configuration, we make use of the following heat source conditions

$$p_1^+ + p_1^- = p_2^+ + p_2^- \qquad \text{(pressure continuity)} \qquad (39)$$

$$\frac{1}{\rho_2 c_2}\left[p_2^+ - p_2^-\right] - \frac{1}{\rho_1 c_1}\left[p_1^+ - p_1^-\right] = \frac{(\gamma-1)}{\rho_1 c_1^2 S}\hat{Q}_f \qquad (40)$$

(velocity jump)

and boundary conditions,
at $x = 0$,

$$p_1^+ = R_0 \, p_1^- \qquad (41)$$

at $x = L$,

$$p_2^- = R_L \, p_2^+ \qquad (42)$$

6.2 Growth rate determination

Equations (39)–(42) can now be written in the form of a matrix equation as

$$[Y(\Omega)]\begin{bmatrix} p_1^+ \\ p_1^- \\ p_2^+ \\ p_2^- \end{bmatrix} = \begin{bmatrix} 0 \\ 0 \\ 0 \\ 0 \end{bmatrix} \qquad (43)$$

with matrix

is solved numerically by Newton-Raphson method or bisection method. The solution, Ω, is a complex quantity of the form $\Omega_m = \omega_m + i\delta_m$, whose real part, ω_m, gives the natural frequency of the mode m, and the imaginary part, δ_m, gives the growth rate. The stability of the mode is determined from the sign of δ_m. Positive δ_m indicates instability and negative δ_m indicates stability.

6.3. Stability maps for various combustor parameters

From equation (45), we can deduce that the parameters which influence the stability of the combustor are: the properties of the medium inside the duct ($\rho_{1,2}$, $c_{1,2}$, $\bar{T}_{1,2}$), the duct length (L), the location of the heat source (l_f), the reflection coefficients at the boundaries (R_0 and R_L), the time-lag (τ) and the heat source coupling coefficient (n). In addition to these parameters, cavity length (l_c), hex dimensions (d and η) and mean flow velocity ($\bar{u}$) in Region 2 have indirect influence through R_L (equation (33)). The R_L also takes into account the influence of the heat sink coefficient (α) and the impedance ratio (ζ_{32}) (using equations (29)–(32) in equation (33)). In this work, however, we examine the influence of frequency, mean flow velocity and cavity length, on the stability of the combustion system.

The stability maps are constructed in the cavity length (l_c)–heat source location (l_f) plane, where the *grey* regions indicate instability and the *white* regions indicate stability. Stability of any mode is determined

$$[Y(\Omega)] = \begin{bmatrix} e^{-i\frac{\Omega}{c_1}l_f} & -R_0 e^{i\frac{\Omega}{c_1}l_f} & 0 & 0 \\ 0 & 0 & R_L e^{i\frac{\Omega}{c_2}(L-l_f)} & e^{-i\frac{\Omega}{c_2}(L-l_f)} \\ 1 & 1 & -1 & -1 \\ -\left(1 + \beta e^{i\Omega\tau}\right) & \left(1 + \beta e^{i\Omega\tau}\right) & \zeta_{12} & -\zeta_{12} \end{bmatrix} \qquad (44)$$

where $\beta = (n(\gamma-1))/(S\rho_1 c_1^2)$ and $\zeta_{12} = (\rho_1 c_1)/(\rho_2 c_2)$.
The characteristic equation, $\det Y(\Omega) = 0$ i.e.

$$\left(1 + \beta e^{i\Omega\tau}\right)\left[-R_L e^{\left(-\frac{i\Omega}{c_1}l_f\right)}e^{\left(\frac{i\Omega}{c_2}(L-l_f)\right)} - e^{\left(-\frac{i\Omega}{c_1}l_f\right)}e^{\left(-\frac{i\Omega}{c_2}(L-l_f)\right)}\right.$$
$$\left. + R_0 R_L e^{\left(\frac{i\Omega}{c_1}l_f\right)}e^{\left(\frac{i\Omega}{c_2}(L-l_f)\right)} + R_0 e^{\left(\frac{i\Omega}{c_1}l_f\right)}e^{\left(-\frac{i\Omega}{c_2}(L-l_f)\right)}\right]$$
$$+ \zeta_{12}\left[R_L e^{\left(-\frac{i\Omega}{c_1}l_f\right)}e^{\left(\frac{i\Omega}{c_2}(L-l_f)\right)} - R_0 e^{\left(\frac{i\Omega}{c_1}l_f\right)}e^{\left(-\frac{i\Omega}{c_2}(L-l_f)\right)}\right]$$
$$- \zeta_{12}\left[e^{\left(-\frac{i\Omega}{c_1}l_f\right)}e^{\left(-\frac{i\Omega}{c_2}(L-l_f)\right)} - R_0 R_L e^{\left(\frac{i\Omega}{c_1}l_f\right)}e^{\left(\frac{i\Omega}{c_2}(L-l_f)\right)}\right] = 0 \qquad (45)$$

from the sign of its growth rate, as mentioned in the previous section. In our study, we look at the stability of the first mode of the combustion system whose properties are listed in Table 2. The cold region is assumed to be at $\bar{T}_1 = 340$ K, with a speed of sound of $c_1 = 370.7$ m/s, and the hot region is assumed to be at $\bar{T}_2 = 1500$ K with a speed of sound of $c_2 = 778.63$ m/s. The duct length L is assumed to be 1 m and the heat source coupling coefficient $n = 187$ kg m/s^2. The time-lag, $\tau = 0.15 \times 10^{-3}$ s, is chosen such that it is much smaller than the fundamental time periods encountered in the stability analysis. A conservative estimate of the time-period range calculated from the stability map is $[\,5.12 \quad 11.95\,] \times 10^{-3}$s.

Firstly, we construct the stability map for mode 1 of the combustor containing only the heat source and no hex, as shown in Figure 12(a). We can observe that the system is unstable for the range of values of l_c and l_f considered. This behaviour can be explained in terms of the mode shape of the wave within the resonator. In the absence of the heat exchanger, the combustor configuration is essentially a quarter-wave resonator with a heat source at $x = l_f$. An increase in cavity length (l_c) effectively adds to the resonator length, L. The total length of the resonator will now be $(L + l_c)$. The first mode shape of the quarter-wave resonator will be, as the name suggests, a quarter wave with a node at $x = 0$ and a maximum at $x = (L + l_c)$. From the Rayleigh criterion, we can conclude this unstable behaviour of the first mode of the resonator, regardless of the cavity length and heat source location considered. Figure 12(b) depicts the eigenfrequency range of the combustion system for the range of values of l_c and l_f considered.

Next, we introduce the heat exchanger with bias flow into the system. The influence of the hex on the stability behaviour of the combustion system can be explained in terms of the parametric analysis given in Section 5. The stability maps are constructed for $\bar{u} = 0.5$, 1.0 and 1.5 m/s, since the numerical simulations for HTF are evaluated only for these velocities. The various $\bar{T}_3$ and ζ_{32} values used for constructing the stability maps are given in Table 1. An increase in the absorption coefficient, Δ_L, is favoured for thermoacoustic instability control because this helps in breaking the feedback loop existing between the acoustic pressure fluctuations and the heat release rate fluctuations.

6.3.1. Influence of frequency (f). Since we calculate the eigenfrequency of the combustion system, frequency cannot be considered as one of the system parameters. However, from Figure 12, we can infer that the increasing l_f values corresponds to the decreasing values of f. Recalling from Section 5.4 that for a given $\bar{u}$, d, η, l_c and ζ_{32}, an increase in f favours the increase in Δ_L, for the frequency range [70–200] Hz. This observation translates to the increase of stability as l_f is decreased.

6.3.2. Influence of cavity length (lc). In terms of the influence of the cavity length, from the results given in Section 5.3, we can conclude that for the given eigenfrequency range and for a given l_c value, higher frequencies will have relatively higher Δ_L compared to the lower frequencies. This augments the effect of l_f on the stability. Also, for the range of eigenfrequencies considered, Δ_L increases as l_c increases. Combining the effects of l_f (or f) and l_c, we expect the stable regions to start appearing from the *right bottom* corner of the stability map. The expected trend for increasing stable

**Table 2.** Properties of the combustion system.

Property	Value
$\bar{T}_1$ (K)	340
c_1 (m/s)	370.7
ρ_1 (kg/m^3)	1.2
$\bar{T}_2$ (K)	1500
c_2 (m/s)	778.63
ρ_2 (kg/m^3)	0.27
L (m)	1
S (m^2)	0.0025
n (kg m/s^2)	187
τ (s)	0.15×10^{-3}
l_f (m)	$[\, 0 \cdots L \,]$
l_c (m)	$[\, 0 \cdots L/2 \,]$
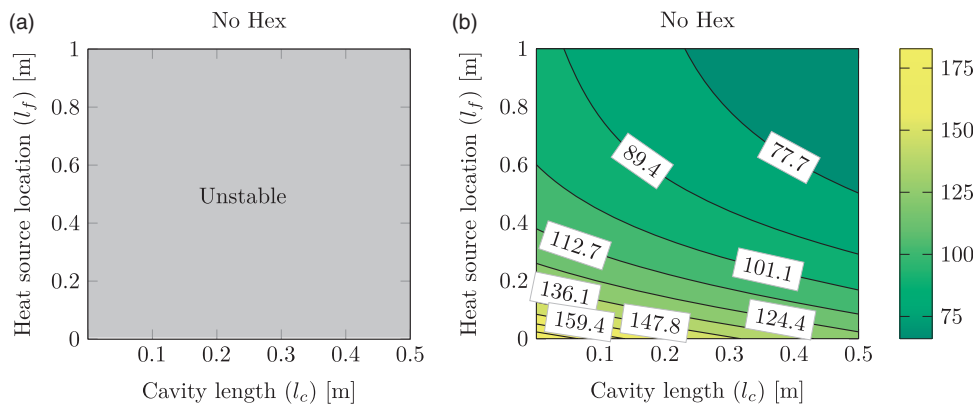
Figure 12. (a) Stability maps obtained for the case without hex and bias flow, and (b) contour map for the eigenfrequencies, ω_1 (in Hz) encountered. The properties of the system are given in Table 2.

regions is shown in Figure 13. This map also includes the effect of the mean flow velocity, as will be discussed in the next section.

6.3.3. Influence of mean flow velocity ($\bar{u}$).
In Section 5.5, we have concluded that an increase in $\bar{u}$ increases the Δ_L and in turn the damping of the unstable mode. Therefore, the stable regions in the stability map *grows* with increasing $\bar{u}$. This growth in the stable region is indicated by the arrow along the diagonal in Figure 13. Therefore, from the parametric analysis, we can expect the overall stability of the combustion system in the $l_f - l_c$ plane, to increase as $\bar{u}$ increases, starting at the right bottom corner. The stability maps constructed for the case with $d = 3$ mm, $\eta = 0.1$ and $\bar{u} = 0.5$, 1.0 and 1.5 m/s, shown in Figure 14, confirms our expected trend for stability growth. Also, there is a range of cavity lengths for a given $\bar{u}$ value where the system is stable irrespective of l_f. This stability and the range of l_c values can be improved further, by increasing $\bar{u}$.
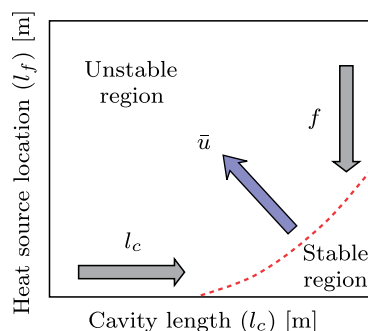
## 6.4. Influence of heat loss and acoustic scattering on stability

As mentioned in Section 3, the response of the hex to upstream velocity fluctuations is modelled as a combination of the heat transfer response and the acoustic scattering response. In this section, the influences of each of these responses are being investigated separately to understand their effects on the stability of the combustion system studied.

6.4.1. Influence of heat loss at hex.
In order to understand the effect of heat losses on the modelled configuration, the stability maps are constructed for the cavity-backed heat sink and no acoustic scattering due to the tube row i.e., $|T_t^\pm| = 1$ and $|R_t^\pm| = 0$.

From Table 1, it can be observed that the temperature of the medium downstream of the heat sink ($\bar{T}_3$) increases with increasing mean velocity $\bar{u}$. This essentially means that the heat absorption capability of the heat sink decreases with increasing velocity. A plausible explanation for this behaviour is that an increase in mean flow velocity increases the mass flow and the heat flow into the domain, while the hex at a constant temperature has a constant surface area for heat absorption. This restriction in the area of absorption (compared to the increase in heat flow) and the reduction in the heat absorbed is manifested as the increase in the outlet temperature.

In the context of the stability of the combustor, the reduction in the heat absorption at the heat sink with increasing $\bar{u}$ leads to an increase in the instability of the system, as can be observed from the plots in Figure 15(a)–(c).

6.4.3. Influence of acoustic scattering (tube row) at hex.
The influence of the tube row or acoustic scattering at hex, in the absence of heat absorption, has already been discussed in Surendran and Heckl.[7,8] They observed

Figure 13. Expected trend for increase in stability, as l_c, l_f and $\bar{u}$ vary.
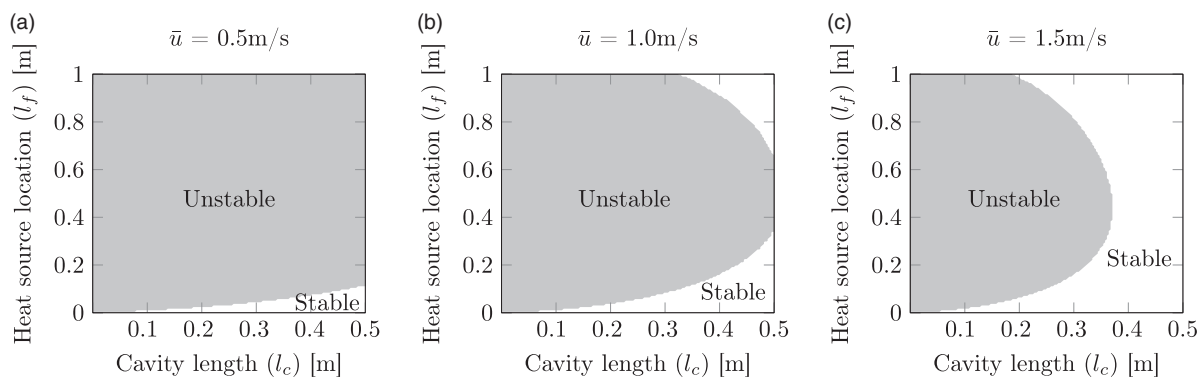
Figure 14. Stability maps obtained for $d = 3$ mm, $\eta = 0.1$ and incoming velocity of (a) $\bar{u} = 0.5$ m/s, (b) $\bar{u} = 1.0$ m/s and (c) $\bar{u} = 1.5$ m/s.
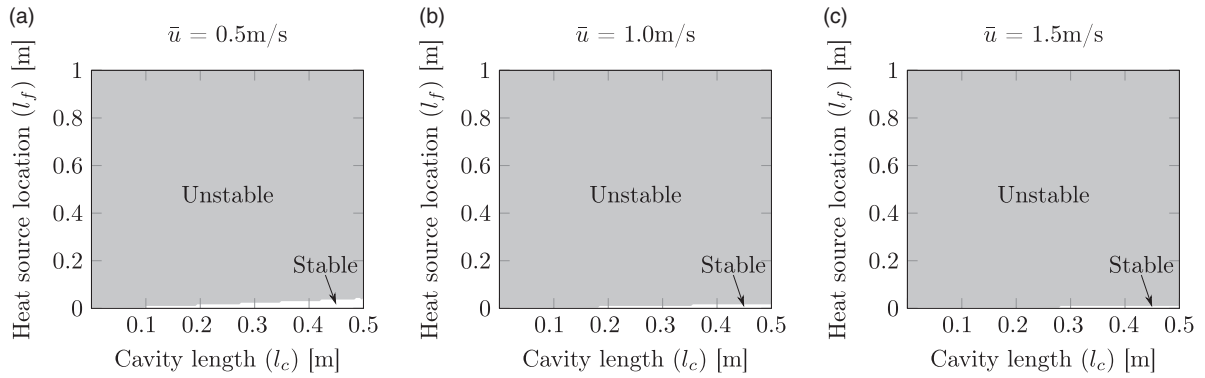
Figure 15. Stability maps obtained for $d = 3$ mm, $\eta = 0.1$ and incoming velocity of (a) $\bar{u} = 0.5$m/s, (b) $\bar{u} = 1.0$m/s and (c) $\bar{u} = 1.5$m/s, in the presence of only the heat sink.
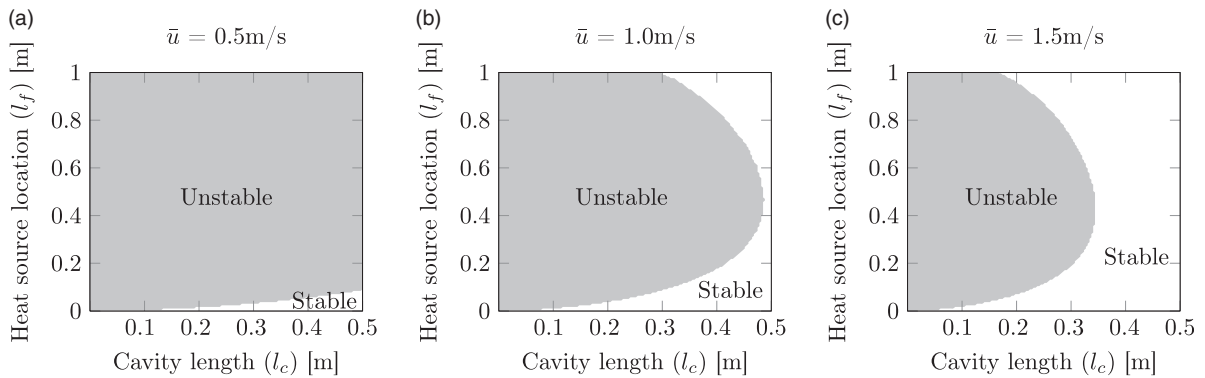
Figure 16. Stability maps obtained for $d = 3$ mm, $\eta = 0.1$ and incoming velocity of (a) $\bar{u} = 0.5$m/s, (b) $\bar{u} = 1.0$m/s and (c) $\bar{u} = 1.5$m/s, in the presence of only the acoustic scatterer.

that in the presence of an acoustic scatterer like a slit-plate[7] or a tube row,[8] an increase in the bias flow velocity (or the incoming velocity) tends to stabilise the combustor. Similar behaviour can be inferred from the stability maps (refer to Figure 16) of our combustor, in the absence of the heat sink. The key mechanism for stabilisation is the vortex dissipation downstream of the tube row.

6.4.4 Influence of hex. The net influence of hex can now be treated as a combination of the influences of the heat sink and the acoustic scattering at the tube row. As $\bar{u}$ increases, the heat sink has a destabilising influence while the scattering at the tube row has a stabilising influence. Figure 14 shows that the overall stability of the system is a balance between these two phenomena. Comparison of Figures 14 and 16 indicate that the stabilising influence of the acoustic scattering dominates over the destabilising influence of the heat sink i.e., in Figure 14, the stability of the system increases with increasing $\bar{u}$, but the stable regions are smaller compared to those in Figure 16.

7. Conclusions

The linear stability analysis of an idealised combustion system with hex is carried out by taking into account the heat absorption and the acoustic scattering at the hex. Using the classical eigenvalue method, the complex eigenfrequencies (Ω_m) of the system are evaluated, by finding the complex roots of the characteristic equation. The sign of the growth rate is an indicator of the stability of the concerned mode, which in our study is the first mode.

The stability maps are constructed in the $l_c - l_f$ plane, and the analysis begins with an already unstable first mode of the combustor (without hex). The combustor, in the absence of the hex, is essentially a quarter-wave resonator with a heat source, whose first mode is always unstable. When hex is introduced near the rigid downstream end, it acts as an acoustic absorber whose reflective (R_L) and absorptive (Δ_L) properties can be varied. These properties depend on the different system parameters like $\bar{u}$, l_c, f, d and η. The aim is to stabilise the system by independently varying one of these parameters, while maintaining the other

parameters as constants. The salient results from our stability analysis are

– We observed that the unstable mode of the combustor can be passively controlled to a large extent by varying the mean flow velocity $\bar{u}$ and the cavity length l_c.
– For an already unstable mode, an increase in velocity tends to stabilise it.
– Similarly, for the rigid downstream end condition ($R_p = 1$), an increase in the cavity length favoured stability.
– Even though frequency cannot be treated as a parameter, the variation in the heat source location l_f manifested as a variation in the eigenfrequencies in the stability maps i.e., as l_f decreased, the $\omega_1 = \Re(\Omega_1)$ increased, and this favours stability.
– The stability maps constructed for the heat sink (alone) shows that stability decreases with increasing $\bar{u}$, while the stability maps for tube row (alone) shows that the stability increases with increasing $\bar{u}$. These plots show that the net influence of the hex on the stability of the combustion system modelled is a combined effect of the heat losses at the heat sink as well as the acoustic energy losses at the tube row due to vortex dissipation.

Our study shows that there is a wide range of values of l_c and $\bar{u}$ that could stabilise a previously unstable mode of the combustor. The practical implications of our findings are promising. It improves the design flexibility of domestic boilers and opens the door to new designs for efficient, clean and reliable boilers and other compact power generation units. One may also choose parameters like the hex tube diameter (d) and the open area ratio (η) to influence the stability behaviour of the combustor.

Declaration of Conflicting Interests

The author(s) declared no potential conflicts of interest with respect to the research, authorship, and/or publication of this article.

References

1. Candel SM. Combustion instabilities coupled by pressure waves and their active control. In: *Twenty-fourth symposium (international) on combustion*, 24 (1992) 1277–1296..
2. McManus KR, Poinsot T and Candel SM. A review of active control of combustion instabilities. *Progr Energy Combust Sci* 1993; 19: 1–29.
3. Lieuwen TC and Yang V. Combustion instabilities in gas turbine engines: operational experience, fundamental mechanisms, and modeling, volume 210 of *Progress in Astronautics and Aeronautics*, American Institute of Aeronautics and Astronautics, Inc., 2005.
4. Kristiansen UR and Fahy FJ. Scattering of acoustic waves by an N-layer periodic grating. *J Sound Vibr* 1972; 24: 315–335.
5. Kristiansen UR and Fahy FJ. Sound propagation and energy dissipation in flow through arrays of small scatterers. *J Sound Vibr* 1974; 32: 189–198.
6. Quinn MC and Howe MS. The influence of mean flow on the acoustic properties of a tube bank. *Proc Math Phys Eng Sci* 1984; 396: 383–403.
7. Surendran A and Heckl MA. Passive instability control by a heat exchanger in a combustor with nonuniform temperature. *Int J Spray Combust Dynam* (2017). Prepublished May 1, 2017.
8. Surendran A and Heckl MA. Passive instability control by using a heat exchanger as acoustic sink. In: *The 22nd international congress on sound and vibration*, July, Florence, Italy, 2015.
9. Munjal ML. *Acoustics of ducts and mufflers – with application to exhaust and ventilation system design*. John Wiley and Sons Ltd, 1987.
10. Dowling AP and Hughes IJ. Sound absorption by a screen with a regular array of slits. *J Sound Vibr* 1992; 156: 387–405.
11. Tran N, Ducruix S and Schuller T. Damping combustion instabilities with perforates at the premixer inlet of a swirled burner. *Proc Combust Instit* 2009; 32: 2917–2924.
12. Tran N, Ducruix S and Schuller T. Passive control of the inlet acoustic boundary of a swirled burner at high amplitude combustion instabilities. *ASME J Eng Gas Turbine Power* 2009; 131: 1–7.
13. Scarpato A, Tran N, Ducruix S, et al. Modeling the damping properties of perforated screens traversed by a bias flow and backed by a cavity at low Strouhal number. *J Sound Vibr* 2012; 331: 276–290.
14. Scarpato A, Ducruix S and Schuller T. A comparison of the damping properties of perforated plates backed by a cavity operating at low and high Strouhal numbers. *Comptes Rendus Mécanique* 2013; 341: 161–170.
15. Heckl M and Kosztin B. Analysis and control of an unstable mode in a combustor with tuneable end condition. *Int J Spray Combust Dynam* 2013; 5: 243–272.
16. Lord Rayleigh. *The theory of sound*. Vol II, 2nd ed. Dover Publications, 1896.
17. Riess P. Das Anblasen offener Röhren durch eine Flamme. *Annalen der Physik und Chemie* 1859; 184: 653-656.

18. Raun RL, Beckstead MW, Finlinson JC, et al. A review of Rjke tubes, Rijke burners and related devices. *Progr Energy Combust Sci* 1993; 19: 313–364.

19. Rigas G, Jamieson NP, Li LKB, et al. Experimental sensitivity analysis and control of thermoacoustic systems. *J Fluid Mech* 2016; 787: R1 1–11.

20. Hosseini N, Teerling OJ, Kornilov V, et al. Thermoacoustic instabilities in a Rijke Tube with heating and cooling elements. In: *Proceedings of the 8th European combustion meeting*, Dubrovnik, Croatia, 2017, pp.3–8.

21. Hosseinalipour SM, Fattahi A and Karimi N. Analytical investigation of non-adiabatic effects on the dynamics of sound reflection and transmission in a combustor. *Appl Thermal Eng* 2016; 98: 553–567.

22. Hosseini N, Kornilov V, Teerling OJ, et al. Transfer function calculations of segregated elements in a simplified slit burner with heat exchanger. In: *The 22nd international congress on sound and vibration*, Florence, Italy, 2015.

23. Witte A, Cabrera A and Polifke W. Identification of the heat transfer frequency response in pulsating laminar and subcritical flow across a cylinder. *J Phys Conf Ser* 2016; 745: 032055/1–8.

24. Strobio Chen L, Witte A and Polifke W. Thermo-acoustic characterization of a heat exchanger in cross flow using compressible and weakly compressible numerical simulation. In: *The 22nd international congress on sound and vibration*, July, Florence, Italy, 2015.

25. Witte A and Polifke W. Dynamics of unsteady heat transfer in pulsating flow across a cylinder. *Int J Heat Mass Transf* 2017; 109: 1111–1131.

26. Lawson CL and Hanson RJ. *Solving least squares problems*. The Society for Industrial and Applied Mathematics, 1995.

27. Ronneberger D. Experimentelle Untersuchungen zum akustischen Reflexionsfaktor von unstetigen Querschnittsänderungen in einem luftdurchströmten Rohr (Experimental investigations about the acoustic reflection coefficient of discontinuous changes of cross-section in tubes with air flow). *Acustica* 1967; 19: 222–235.

28. Hofmans GCJ, Boot RJJ, Durrieu PPJM, et al. Aeroacoustics response of a slit-shaped diaphragm in a pipe at low Helmholtz number, 1: Quasi-steady results. *J Sound Vibr* 2001; 244: 35–56.

29. Hofmans GCJ, Groot G, Ranucci M, et al. Unsteady flow through in-vitro models of the glottis. *J Acoust Soc Am* 2003; 113: 1658–1675.

30. Durrieu P, Hofmans G, Ajello G, et al. Quasisteady aeroacoustic response of orifices. *J Acoust Soc Am* 2001; 110: 1859–1872.

31. Hofmans GCJ. *Vortex sound in confined flows*. PhD Thesis, Technische Universiteit, Eindhoven, 1998.

32. Surendran A, Heckl MA, Boij S, et al. Aeroacoustic response of an array of tubes with bias-flow. In: *The 23rd international congress on sound and vibration*, July, Athens, Greece, 2016.

33. Surendran A. *Passive control of thermoacoustic instabilities in idealised combustion systems using heat exchangers*. PhD Thesis, Keele University, 2017.

34. Strobio Chen L, Polifke W, Hosseini N, et al. Acoustic scattering behaviour of a 2D flame with heat exchanger in cross-flow. In: *The 23rd international congress on sound and vibration*, July, Athens, Greece, 2016.

35. Surendran A and Heckl MA. Analytical study of a Rijke tube with heat exchanger. In: *The 21st international congress on sound and vibration*, Beijing, China, 2014.